THE PENNSYLVANIA STATE UNIVERSITY
SCHREYER HONORS COLLEGE

DEPARTMENT OF BIOENGINEERING

MODELING THE ROLL-SLIP NONLINEAR DYNAMICS OF THE KNEE

VIRGINIA M. GAGLIARDI

Spring 2010

A thesis
submitted in partial fulfillment
of the requirements for a baccalaureate degree
in Bioengineering
with honors in Bioengineering

Reviewed and approved* by the following:

Joseph P. Cusumano
Professor of Engineering Science and Mechanics
Thesis Supervisor

William O. Hancock
Associate Professor of Bioengineering
Honors Adviser

Margaret J. Slattery
Assistant Professor of Bioengineering
Faculty Reader

* Signatures are on file in the Schreyer Honors College.

ABSTRACT

A better understanding of the cause and effect of various knee injuries as well as the design and optimization of more environmentally-adaptive knee prostheses are becoming a great need throughout all of society, yet the fundamental dynamics within the knee joint itself are not well-understood. The aim of this study was to mathematically model the roll-slip nonlinear dynamics of the knee joint in order to observe and to quantify the motions of the knee. A spring-mass-damper, rolling disk on flat surface model was analyzed mathematically using MATLAB®. The results obtained showed preliminary insight into the dynamics occurring within the knee joint. Specifically, as the static coefficient of friction increased within the knee, slipping decreased leading to increased steady state response and average power amplitudes. Therefore, a static coefficient of friction that is approximately equal to the kinetic coefficient of friction within the knee provides appropriate levels of slipping and decreased wear on the system. Adequate slipping is a key dynamical component in the motion of the knee; too little or too much slipping within the knee would result in increased instability and could potentially lead to injury of the soft tissues within the joint.

TABLE OF CONTENTS

LIST OF FIGURES

ACKNOWLEDGEMENTS

I would like to thank Dr. Cusumano for being my thesis supervisor and a mentor to me academically for the past three years. I greatly appreciate the knowledge he has shared with me and the patience he has shown while teaching. I would also like to thank Arjun Roy, who has been ever-willing to help me throughout this year and has offered his good advice in much of my work; and Joby John, who started me on this journey several years ago. In addition, I would like to thank Dr. Hancock, my honors adviser, and Dr. Slattery for their support and for serving as part of my thesis committee. Lastly, I want to thank my friends and family, especially my mom who has kept me motivated and has been a source of inspiration to me not only through this tough year, but throughout my whole life. I am where I am today, and I am who I am today, because of her.

Chapter 1

Introduction

1.1. Introduction to the knee

The knee is a complex joint which creates motions that are not very well understood [1]. Although commonly mistaken for a pure hinge-joint, the six degrees of freedom within the joint [2] cause it to take on motion of a modified-hinge joint, rather than a true hinge. This characteristic of the knee joint is what leads to the complexity of its analysis, as well as to the ambiguity surrounding its dynamics [1, 3].

1.1.1. Structure of the knee joint

A joint is the location where the ends of two bones meet, muscles and soft tissues cross, and considerable motion is exhibited [4]. The knee joint in particular, displayed in Figure 1-1 [5], is where the femur meets the tibia [6]. Comprising the knee joint are two interdependent joints—the patellofemoral joint and the tibiofemoral joint. In the patellofemoral joint, the patellar ligament anchors the patella to the tibia and works in conjunction with the quadriceps tendon to allow the patella to smoothly glide over the anterior surface of the femur during motion [7]. The tibiofemoral joint consists of the junction of the femur and tibia. Separating the two bones are the menisci, concave disks of cartilage which allow smooth articulation of the convex distal condyles of the femur on the tibial plateau [6]. The concavity of the menisci aids in neutralizing the joint

instability caused by the convex condyles of the femur articulating on the flat surface of the tibial plateau [7].

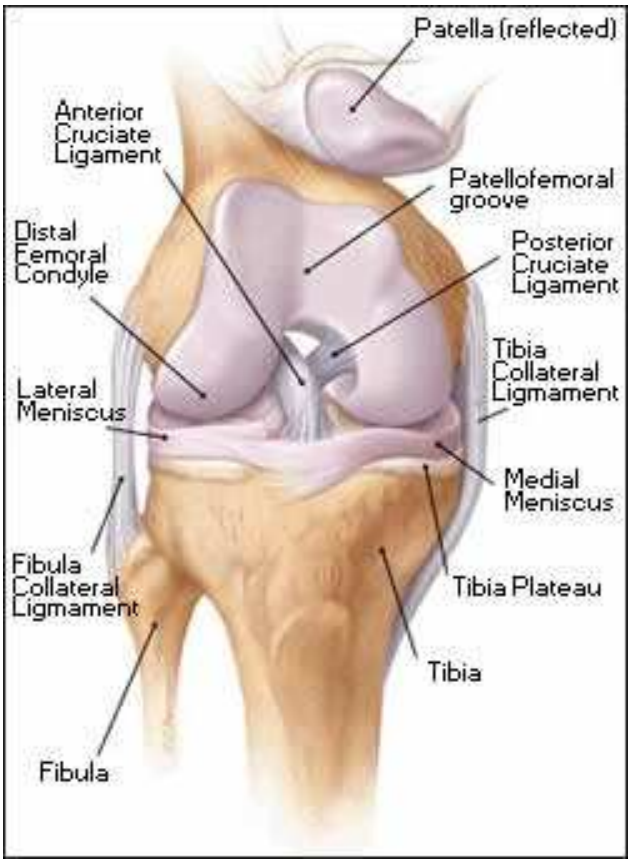

Figure 1-1: Anatomical structure of the knee joint.
Christy Krames., *Knee Joint*.
http://www.orthopaedics.co.uk/boc/patients/knee_arthritis_intro.htm

The ligaments within the tibiofemoral joint also contribute to joint stabilization. The anterior cruciate ligament (ACL) and posterior cruciate ligament (PCL) are within the knee joint. The ACL connects the anterior tibial plateau to the femur while the PCL connects the posterior tibial plateau to the femur. The lateral collateral ligament (LCL) and medial collateral ligament (MCL) are on the lateral and medial external portions of the joint, respectively. The LCL connects the lateral epicondyle of the femur to the

lateral portion of the fibular head, while the MCL connects the medial epicondyle of the femur to the medial portion of the tibial head [7].

1.1.2. Functions of and within the knee joint

The two main functions of the entire knee joint are extension and flexion of the knee. Within these motions, the joint experiences two phases: a rolling-only phase and a roll-slide phase. In flexion, the rolling-only phase appears first, followed by the roll-slide phase. Conversely in extension, the order is reversed [7]. Other translational and rotational motions are also possible within the knee, due to the structural characteristics of the tibiofemoral joint [8]. The tissue components of the joint, though, work to reduce these effects.

The lateral and medial menisci have four main functions within the knee joint. First, the menisci work to absorb shock translated through the joint. They also aid in maintaining the synovial fluid contained within the joint throughout the cartilage via its sponge-like structure. The synovial fluid is extremely slippery and acts as a friction mitigator within the joint [3]. In addition, the menisci help to provide normal movement between the articular surfaces of the femur and tibia, as well as to maintain congruity between the two surfaces throughout all of the joint [7]. More specifically as stated by Watkins:

> …during joint movement the menisci deform in response to the changing curvature of the femoral condyles and thus maintain congruence between the articular surfaces in all positions of the joint. The increase in congruence

provided by the menisci results in increased joint stability and also minimizes the compressive stress on the articular cartilages [7].

The ligaments of the knee operate together in order to stabilize the joint. The PCL and ACL work intimately within the joint to prevent rotational and translational movements. The PCL prevents posterior dislocation of the tibia under the femur. The ACL prevents forward dislocation of the tibia under the femur while also providing rotational stability. The MCL prevents the knee from abducting while the LCL prevents adduction [9]. Due to the cooperation between the cruciate and collateral ligaments of the knee, an injury to any one of these ligaments causes instability within the joint and increases the chance of damage to the menisci [7].

1.2. Previous analyses on roll-slide oscillators

While the knee joint is still not well understood, some researchers have tried to quantify its dynamics. With the knee defined by rolling and sliding motions, research regarding roll-slide oscillators is pertinent to characterizing the nonlinear dynamics of the knee. The works of two main research groups were cited for justification of the dynamical analysis in this study.

1.2.1. Dynamical Findings of Awrejcewicz and Someya

The work of Awrejcewicz and Someya in “A Twisted Horseshoe in the Roll-Slide Oscillator” focused on the chaotic behavior arising from the nonlinear dynamics of a roll-

slide system. The study performed was an in-depth analysis of their specific system involving the periodic orbits arising within and their classifications as attractor or repelling orbits. In the analysis, the orbits were investigated as they approached each other. The result was the formation of a chaotic attractor within the orbits. Though the model of interest is different than that studied in the work of Awrejcewicz and Someya, their analysis of a roll-slide oscillator resulted in complicated dynamics including periodic orbits and even chaos [10]. It was noted that since the knee is a roll-slide oscillator, the range of dynamical behaviors should be similar to those observed in this classification of systems.

1.2.2. Model by Schwenke, Borgstede, Schneider, Andriacchi, and Wimmer

The work of Schwenke, et al. in "The influence of slip velocity on wear of total knee arthroplasty" focused on the generation of wear in total knee replacements. Their methodology involved a chromium wheel-on-flat (WOF) simulator design, with the ultra-high-molecular-weight-polyethylene (UHMWPE) flat portion containing the oscillatory feature of the roll-slide oscillator system as shown in Figure 1-2 [11]. By applying axial force loads to the WOF system, slip velocity data was gathered as it related to wear within the system. The results demonstrated that at high slip velocities during rolling or roll-to-slip transitions, the highest amount of wear was generated in the WOF model. It was noted that the system involved a rolling wheel on an oscillating flat surface to generate these results, which was pertinent to establishing the validity of the model proposed in this study [11] and predictions for parameters of interest .

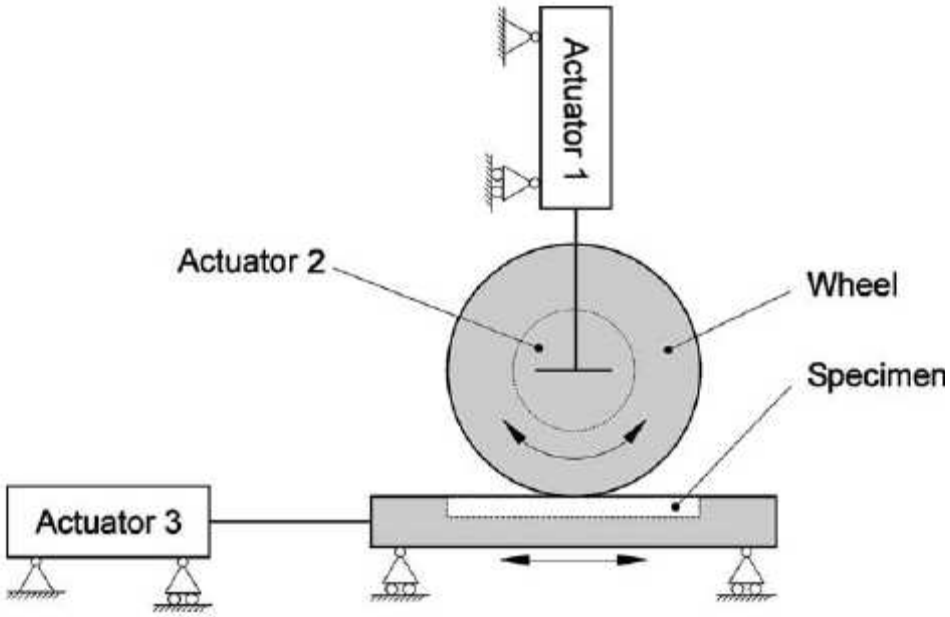

Figure 1-2**:** Wheel-on-flat simulator for the roll-slide oscillator system.
Schwenke, T., Borgstede, L. L., Schneider, E., Andriacchi, T. P., and Wimmer, M. A., 2005, "The influence of slip velocity on wear of total knee arthroplasty," Wear, 259, pp. 926-932.

1.3. Contribution of this study

Because of the complexity and ambiguity associated with the knee joint, this study aims to explore and quantify the motions associated with it. Overall it will aim to provide more information on the behaviors of the knee observed clinically. Should the data produced in this study demonstrate chaotic behaviors, significant implications in both the real and artificial knees could be noted.

1.3.1. Implications in the real knee

With regard to the real knee, the resulting data and potential for the formation of chaos could supply a better understanding of the high incidence of certain knee injuries—such as ACL tears—which maintain origins that are not well known currently, but cause an increase in the frictional dynamics of the joint [3]. The results could also provide more insight into the high incidence of knee injuries in females [12] and other similar, seemingly unexplainable phenomena.

1.3.2. Implications in the prosthetic knee

Similarly to the real knee, the resulting data from this study will provide more insight into the prosthetic knee and its motions observed clinically. This is imperative as more electronic and more precise prostheses are designed. In addition, if chaotic behavior is found to exist through future, more in-depth analysis of the system, the result could aid the design of the environmentally-adaptive prosthetic knee [13] in order to incorporate the avoidance of a chaotic threshold and to maintain the biological realism of movements. While some newer prosthetic knee joints have been designed with safety in mind, many current and previous designs contain unknown dynamics [14] and carry a high risk of injury, such as falls [15]. By exploring the nonlinear dynamics of the knee in this study, the motions of the knee could be better quantified and could be applied to innovative prosthetic design.

Chapter 2

Materials and Methods

2.1. Spring-tensioned, damped rolling disk on flat surface with forcing

The model, depicted in Figure 2-1, was designed as a rolling disk on a flat surface, where *L* represents the unstretched length of the spring, *k* represents the stiffness of the spring, *c* represents the damping of the system, and *F* is an oscillatory force. The spring and damping forces opposing the oscillatory force were added to the system to simulate the roll-slip dynamics associated with the knee.

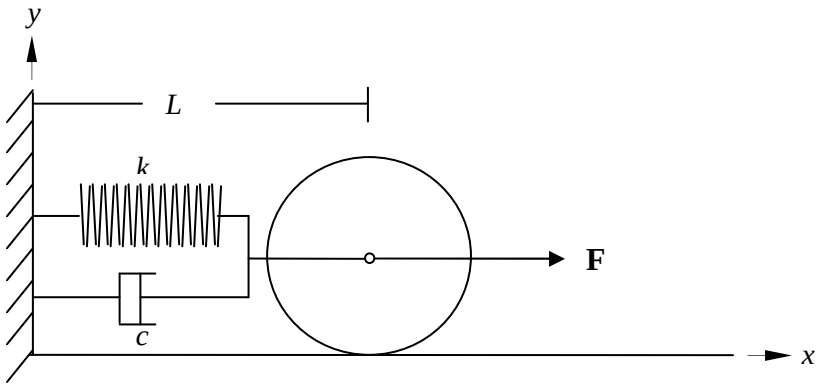

Figure 2-1: Model of rolling disk on flat surface. The elements shown include the spring constant *k*, damping element *c*, forcing *F*, and unstretched spring length *L*.

2.1.1. Justification and validity of model

The structure of the model was chosen due to the convex femoral condyles, the disk, articulating on the flat tibial plateau, the flat surface in the model. This model neglects the concavity of the menisci in order to explore the basic dynamics occurring

within the system. The validity of this assumption was also confirmed by the WOF system utilized by Schwenke, et al. [11]. In addition, given the damping and resistive properties of the ligaments and tendons in the joint [16], a single spring and a single damper were applied to the model to supply tension and damping to the system as a model for the soft tissues. An oscillatory force was also applied to the disk to signify the periodic motions of gait [17].

2.1.2. Equations of motion

A force analysis was first done on the model for rolling conditions to determine the rolling kinetics, as shown in Figure 2-2, where on the left-hand side F_s is the spring force, F_c is the damping force, $F(t)$ is the forcing, mg is the weight of the disk, R is the radius of the disk, N is the normal force acting on the disk, C is the point of contact, and P is the contact force experienced by the disk. On the right-hand side of Figure 2-2, I represents the inertia of the disk, $\ddot{\theta}$ represents the angular acceleration of the disk, m represents the mass of the disk, and $\ddot{x}$ represents translational acceleration of the disk. Similarly, Figure 2-3 displays the slipping kinetics, where frictional force F_f is experienced by the disk. The equations of motion were then generated in accordance with principles derived from dynamic theory [18].

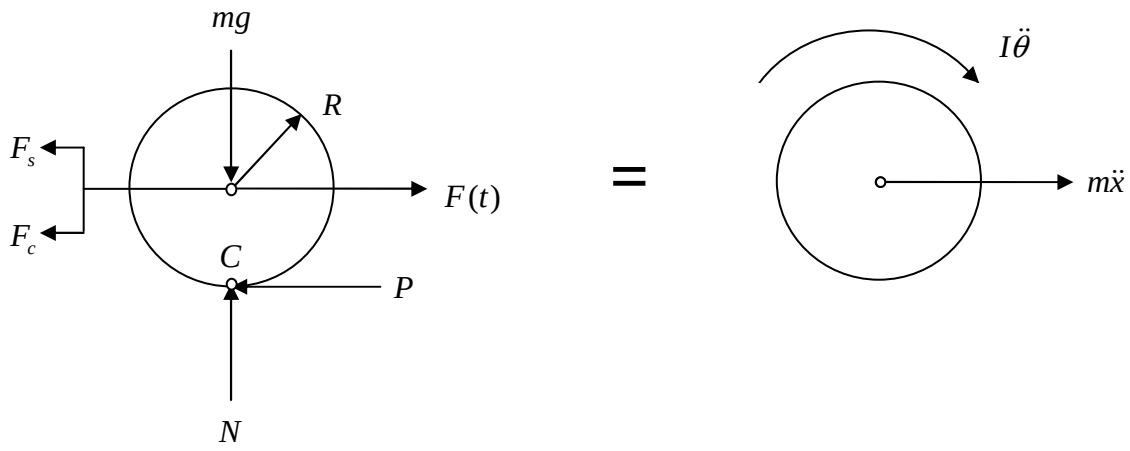

Figure 2-2: Rolling kinetics. The spring force F_s, damping force F_c, forcing function $F(t)$, contact force P, and normal force N acting on the disk of radius R and weight mg shown on the left hand side. The equivalent linear and angular motions, $m\ddot{x}$ and $I\ddot{\theta}$, respectively, of the disk are shown on the right hand side.

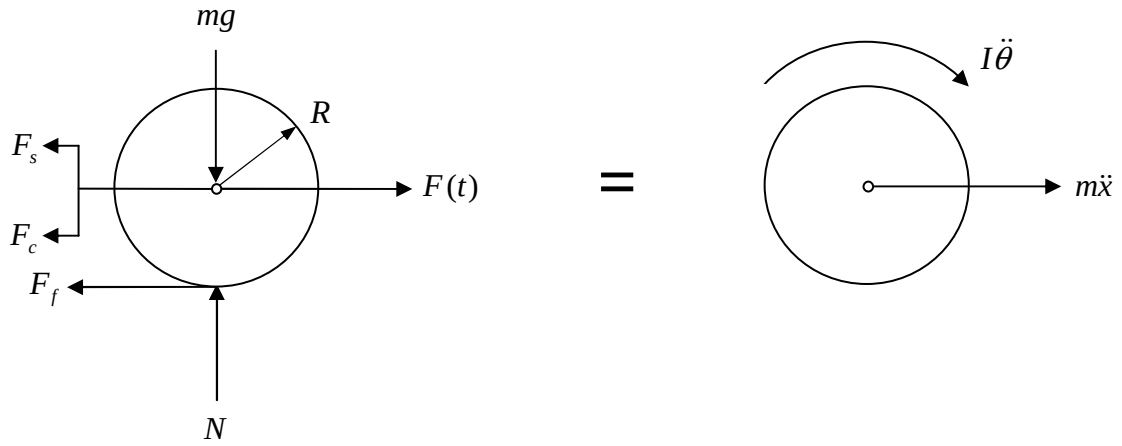

Figure 2-3: Slipping kinetics. The spring force F_s, damping force F_c, forcing function $F(t)$, frictional force F_f, and normal force N acting on the disk of radius R and weight mg shown on the left hand side. The equivalent linear and angular motions, $m\ddot{x}$ and $I\ddot{\theta}$, respectively, of the disk are shown on the right hand side.

Utilizing the equations of motion for forces in equation (1) and for moments in equation (2) [18], the forces of the rolling condition within the model were analyzed

$$\sum F = ma \tag{1}$$

$$\sum M = I\alpha \tag{2}$$

where $a = \ddot{x}$ and $\alpha = \ddot{\theta}$. Resolving the normal (N) and weight (mg) forces in the y-direction yielded equation (3).

$$N = mg \tag{3}$$

Resolving the spring (F_s), damping (F_c), oscillatory ($F(t)$), and contact (P) forces with respect to the mass (m) and linear acceleration (a) of the disk in the x-direction determined equation (4), where $F_s = k(x - L)$, the product of the spring constant (k) and the displacement by the spring from its original length, L *and* $F_c = c\dot{x}$, the product of the value of damping (c) and the rate of displacement ($\dot{x}$). Since the disk is rolling, the velocity (v_c) at the point of contact, C, is zero such that the velocity (v_g) at the center of the disk ($\dot{x}$) and the velocity ($v_{c/g}$) at C with respect to the center of the disk ($-R\dot{\theta}$) are equal, as shown in equation (5).

$$F(t) - F_c - F_s - P = F(t) - c\dot{x} - k(x - L) - P = m\ddot{x} \tag{4}$$

$$v_c = v_g + v_{c/g} = \dot{x} - R\dot{\theta} = 0 \tag{5}$$

The moment (M) generated by the contact force P a radial distance R from the center of the disk analyzed with the moment of inertia (I) and angular acceleration ($\ddot{\theta}$) generated by rolling gave equation (6).

$$M = RP = I\ddot{\theta} \tag{6}$$

Similarly, the force and moment analysis were performed for the slipping conditions of the disk. Resolving the normal (N) and weight (mg) forces in the y-direction yielded equation (7).

$$N = mg \tag{7}$$

Resolving the spring (F_s), damping (F_c), oscillatory ($F(t)$), and friction (F_f) forces with respect to the mass (m) and linear acceleration (a) of the disk in the x-direction determined equation (8), where $F_f = \mu_k N sgn(v_c)$, the product of the coefficient of friction (μ_k) and the normal force ($N=mg$) whose direction is determined by the sign of the velocity at the point of contact, C. Equation (9) gives the velocity at C (v_c) with respect to the velocity at the center of the disk ($\dot{x}$) and the velocity at C with respect to the center of the disk ($-R\dot{\theta}$).

$$F(t) - F_c - F_s - F_f = F(t) - c\dot{x} - k(x - L) - \mu_k mg\,\mathrm{sgn}(v_c) = m\ddot{x} \tag{8}$$

$$v_c = \dot{x} - R\dot{\theta} \tag{9}$$

The moment (M) generated by the friction force F_f a radial distance R from the center of the disk analyzed with the moment of inertia (I) and angular acceleration ($\ddot{\theta}$) generated by slipping gave equation (10).

$$M = RF_f = R\mu_k mg\,\mathrm{sgn}(v_c) = I\ddot{\theta} \tag{10}$$

Therefore, in defining the movement of the disk in terms of v_c, rolling is given by equation (11), while slipping is given by equation (12).

$$v_c = 0 \tag{11}$$

$$v_c \neq 0 \tag{12}$$

Furthermore, when $v_c = 0$, the governing equations for rolling follow equations (13a) and (13b), where P is governed by equation (14) for rolling conditions where μ_S represents the static coefficient of friction which must be overcome by the contact force, P, in order for slipping to occur.

$$m\ddot{x} + c\dot{x} + k(x - L) = -P + F(t) \tag{13a}$$

$$I\ddot{\theta} = RP \tag{13b}$$

$$P = \frac{I}{R^2}\left[\frac{F(t) - k(x - L) - c\dot{x}}{m + \frac{I}{R^2}}\right] \leq \mu_s mg \tag{14}$$

For $v_c > 0$, the result is slipping in the positive x-direction governed by equations (15a) and (15b). For $v_c < 0$, the result is slipping in the negative x-direction governed by equations (16a) and (16b).

$$m\ddot{x} + c\dot{x} + k(x - L) + \mu_k mg = F(t) \tag{15a}$$

$$I\ddot{\theta} - \mu_k mgR = 0 \tag{15b}$$

$$m\ddot{x} + c\dot{x} + k(x - L) - \mu_k mg = F(t) \tag{16a}$$

$$I\ddot{\theta} + \mu_k mgR = 0 \tag{16b}$$

A non-dimensional analysis was also performed on the equations for both the rolling and slipping conditions. The substitution of $u = \frac{x}{L} - 1$ and $\tau = \sqrt{\frac{k}{m}}t$ into the governing equations with rearrangement and $\omega = \sqrt{\frac{m}{k}}$, the frequency of forcing, yields equation set (17) for rolling

$$\left(m + \frac{I}{R^2}\right)\frac{kL}{m}u'' + c\sqrt{\frac{k}{m}}Lu' + kLu = F(\omega\tau) \tag{17a}$$

$$I\left(\frac{k}{m}\right)\theta'' = RP = \frac{I}{R}\left[\frac{F(\omega\tau) - c\sqrt{\frac{k}{m}}Lu' - kLu}{m + \frac{I}{R^2}}\right] \tag{17b}$$

and equation sets (18) and (19) for positive and negative slipping, respectively.

$$m\left(\frac{k}{m}\right)Lu'' + c\sqrt{\frac{k}{m}}Lu' + kLu + \mu_k mg = F(\omega\tau) \tag{18a}$$

$$I\left(\frac{k}{m}\right)\theta'' - \mu_k mgR = 0 \tag{18b}$$

$$m\left(\frac{k}{m}\right)Lu'' + c\sqrt{\frac{k}{m}}Lu' + kLu - \mu_k mg = F(\omega\tau) \tag{19a}$$

$$I\left(\frac{k}{m}\right)\theta'' + \mu_k mgR = 0 \tag{19b}$$

By defining non-dimensional parameters, the rolling equations become

$$u'' + d \cdot u' + \gamma \cdot u = \gamma \cdot f(\omega\tau) \tag{20a}$$

$$\theta'' = \frac{u''}{R} \tag{20b}$$

while the positive and negative slipping equations, respectively, become

$$u'' + au' + u + \mu_k \alpha = f(\omega\tau) \tag{21a}$$

$$\theta'' - \mu_k \beta = 0 \tag{21b}$$

$$u'' + au' + u - \mu_k \alpha = f(\omega\tau) \tag{22a}$$

$$\theta'' + \mu_k \beta = 0 \tag{22b}$$

where

$$f(\omega\tau) = f_m \sin(\omega\tau) \tag{23}$$

$$\alpha = \frac{mg}{kL} \tag{24}$$

$$\beta = \frac{m^2 gR}{kI} \tag{25}$$

$$\gamma = \frac{mR^2}{I + mR^2} \tag{26}$$

$$a = \frac{c}{\sqrt{km}} \tag{27}$$

$$d = \frac{c\gamma}{\sqrt{km}} \tag{28}$$

for both the slipping and the rolling conditions.

2.1.3. Analytical Analysis

The roll-slip model was first solved analytically in a manner derived from Feeny and Moon's analysis of a stick-slip oscillator [19]. The analytical solution [20] for the translational and angular position, respectively, during rolling resulted in the following:

$$u = A\exp\left(\frac{-\pi d}{2\sqrt{\gamma}}\right)\sin(e\sqrt{\gamma}\tau + \psi) + u_{r1}\sin\omega_f\tau + u_{r2}\cos\omega_f\tau \tag{29a}$$

$$\theta = l(u - u_{r0}) + \theta_{r0} \tag{29b}$$

$$u_{r1} = \frac{\gamma f_m(\gamma - \omega_f^2)}{[(\gamma - \omega_f^2)^2 + (\omega_f d)^2]} \tag{30}$$

$$u_{r2} = \frac{-\gamma\omega_f f_m d}{[(\gamma - \omega_f^2)^2 + (\omega_f d)^2]} \tag{31}$$

$$e = \sqrt{1 - \frac{d^2}{4\gamma}} \tag{32}$$

$$l = \frac{L}{R} \tag{33}$$

where constants A and ψ are determined from initial conditions:

$$A = \sqrt{R_1^2 + R_2^2} \tag{34}$$

$$\psi = \tan^{-1}\left(\frac{R_1}{R_2}\right) - e\sqrt{\gamma}\tau_{st} \tag{35}$$

and

$$R_1 = \exp\left(\frac{\tau_{st} d}{2\sqrt{\gamma}}\right)\left[u_{r0} - u_{r1}\sin\omega_f\tau_{st} - u_{r2}\cos\omega_f\tau_{st}\right] \tag{36}$$

$$R_2 = \frac{\exp\left(\frac{\tau_{st} d}{2\sqrt{\gamma}}\right)}{e\sqrt{\gamma}}\left[\begin{array}{l} v_{r0} - u_{r1}\omega_f\cos\omega_f\tau_{st} + u_{r2}\omega_f\sin\omega_f\tau_{st} \\ + \frac{d}{2\sqrt{\gamma}}\left(u_{r0} - u_{r1}\sin\omega_f\tau_{st} - u_{r2}\cos\omega_f\tau_{st}\right) \end{array}\right] \tag{37}$$

with u_{r0}, v_{r0}, and θ_{r0} as the initial rolling conditions for displacement, velocity, and angular position, respectively, and τ_{st} representing the time that rolling starts.

The solutions for the translational and angular position, respectively, during positive slipping are as follows:

$$u = B\exp\left(\frac{-a\tau}{2}\right)\sin(b\tau + \phi) + u_{p1}\sin\omega_f\tau + u_{p2}\cos\omega_f\tau - \mu_k\alpha \tag{38a}$$

$$\theta = \theta_{01} + \theta_{02}(\tau - \tau_s) + \frac{\mu_k\beta}{2}(\tau - \tau_s)^2 \tag{38b}$$

$$u_{p1} = \frac{f_m(1-\omega_f^2)}{\left[(1-\omega_f^2)^2 + (\omega_f a)^2\right]} \tag{39}$$

$$u_{p2} = \frac{-a\omega_f f_m}{\left[(1-\omega_f^2)^2 + (\omega_f a)^2\right]} \tag{40}$$

$$b = \sqrt{1 - \frac{a^2}{4}} \tag{41}$$

where constants B and ϕ are determined from initial conditions:

$$B = \sqrt{R_3^2 + R_4^2} \tag{42}$$

$$\phi = \tan^{-1}\left(\frac{R_3}{R_4}\right) - b\tau_s \tag{43}$$

and

$$R_3 = \exp\left(\frac{a\tau_s}{2}\right)\left[u_0 - u_{p1}\sin\omega_f\tau_s - u_{p2}\cos\omega_f\tau_s + \mu_k\alpha\right] \tag{44}$$

$$R_4 = \frac{\exp\left(\frac{a\tau_s}{2}\right)}{b}\left[\begin{array}{l} v_0 - u_{p1}\omega_f\cos\omega_f\tau_s + u_{p2}\omega_f\sin\omega_f\tau_s \\ + \frac{a}{2}\left(u_0 - u_{p1}\sin\omega_f\tau_s - u_{p2}\cos\omega_f\tau_s + \mu_k\alpha\right) \end{array}\right] \tag{45}$$

with u_0, v_0, θ_{01}, and θ_{02} as the initial slipping conditions for displacement, velocity, angular position, and angular velocity, respectively, and τ_s representing the time that slipping starts.

The solutions for the translational and angular position, respectively, during negative slipping resulted in:

$$u = B\exp\left(\frac{-a\tau}{2}\right)\sin(b\tau + \phi) + u_{p1}\sin\omega_f\tau + u_{p2}\cos\omega_f\tau + \mu_k\alpha \tag{46a}$$

$$\theta = \theta_{01} + \theta_{02}(\tau - \tau_s) - \frac{\mu_k\beta}{2}(\tau - \tau_s)^2 \tag{46b}$$

where constants B and ϕ are determined from initial conditions as shown in equations (42) and (43), respectively, according to the following:

$$R_3 = \exp\left(\frac{a\tau_s}{2}\right)\left[u_0 - u_{p1}\sin\omega_f\tau_s - u_{p2}\cos\omega_f\tau_s - \mu_k\alpha\right] \tag{47}$$

$$R_4 = \frac{\exp\left(\frac{a\tau_s}{2}\right)}{b}\left[\begin{array}{l} v_0 - u_{p1}\omega_f \cos\omega_f\tau_s + u_{p2}\omega_f \sin\omega_f\tau_s \\ + \frac{a}{2}\left(u_0 - u_{p1}\sin\omega_f\tau_s - u_{p2}\cos\omega_f\tau_s - \mu_k\alpha\right) \end{array}\right] \tag{48}$$

Utilizing the solutions, the slip-roll boundary was determined citing the method used by Feeny and Moon [19]. The slip-roll boundary is shown in Figure 2-4 and is given by

$$\frac{-\mu_k\alpha}{(1-\gamma)} \le \left[\begin{array}{l} A\exp\left(\frac{-\pi d}{2\sqrt{\gamma}}\right)\sin(e\sqrt{\gamma}\tau+\psi) + u_{r1}\sin\omega_f\tau + u_{r2}\cos\omega_f\tau \\ + \frac{Ad}{\gamma}\left[\begin{array}{l} \frac{-d}{2\sqrt{\gamma}}\exp\left(\frac{-\pi d}{2\sqrt{\gamma}}\right)\sin(e\sqrt{\gamma}\tau+\psi) \\ + e\sqrt{\gamma}\exp\left(\frac{-\pi d}{2\sqrt{\gamma}}\right)\cos(e\sqrt{\gamma}\tau+\psi) \end{array}\right] \\ + \frac{d\omega_f}{\gamma}u_{r1}\cos\omega_f\tau - \frac{d\omega_f}{\gamma}u_{r2}\sin\omega_f\tau - f_m\sin\omega_f\tau \end{array}\right] \le \frac{\mu_k\alpha}{(1-\gamma)} \tag{49}$$

representing the rolling region—the inside portion of the inequality—bounded by regions of positive and negative slip on the left- and right-hand sides of the inequality, respectively.

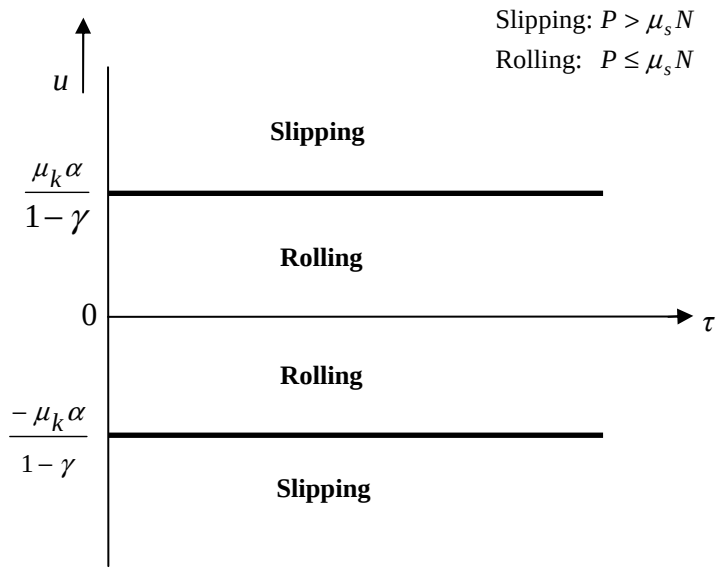

Figure 2-4: Graphical representation of slip-roll boundaries and rolling and slipping regions. Slipping and rolling are governed by the value of the contact force *P* with respect to the product of the static coefficient of friction μ_s and the normal force *N*.

2.1.4. Numerical Analysis

After solving the rolling and slipping conditions analytically, a numerical analysis was performed on the model using MATLAB®, a technical computing software solution [21]. A code logic and algorithm created by Arjun Roy [22] was utilized, with the code logic used to produce the algorithm included in Appendix A. The algorithm was run by applying biologically realistic values for the parameters deemed most important to this study—the static and kinetic coefficients of friction—while holding the other values including the forcing, damping factor, spring constant, radius of the disk, weight of the disk, and the unstretched length of the spring constant. The value used for the kinetic

coefficient of friction was μ_k=0.003, whereas the values of the static coefficient of friction were varied from μ_s=0.004 to μ_s=0.01 [23].

Chapter 3

Results and Discussion

3.1. Results of spring-tensioned, damped rolling disk on flat surface with forcing

Utilizing the equations of solution as well as the MATLAB® code, analysis was performed on the spring-mass-damper system. The code was previously validated to verify its accuracy by comparing typical results with those expected from known systems. It was then used to generate plots of the dynamical responses of the spring-tensioned, damped rolling disk on flat surface model. The results from the system were then discussed in terms of their significance within the system.

3.1.1. Results

To demonstrate the rolling characteristics of the system, a simulation using a specified value of frequency was run on the model. The results for a typical rolling solution for μ_s=0.01 and ω=0.83 rad/s are shown in Figure 3-1. Similarly, the roll-slip characteristics of the system were simulated for μ_s=0.01 and ω=0.8315 rad/s. The typical roll-slip result is shown in Figure 3-2.

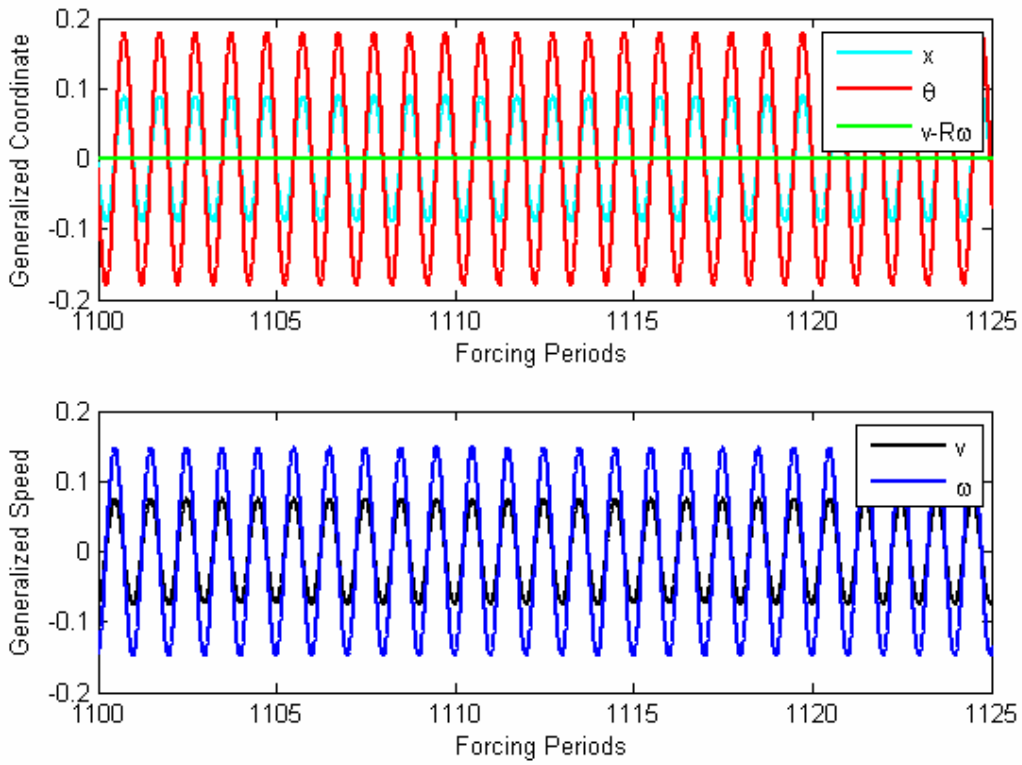

Figure 3-1: The typical rolling result for the model. In this case, the mass was set to m=1 kg, the damping was set to c=0.003 N-s/m, the spring constant was set to k=1 N/m, the amplitude of the forcing was set to F=0.003 N, the unstretched spring length was set to L=1 m, the radius of the disk was set to R=0.5 m, the static coefficient of friction was set to μ_s=0.01, the kinetic coefficient of friction was set to μ_k=0.003, and the forcing frequency was set to ω=0.83 rad/s. The simulation was run for 1400 forcing periods, with the first 1000 discarded to avoid transients in analysis.

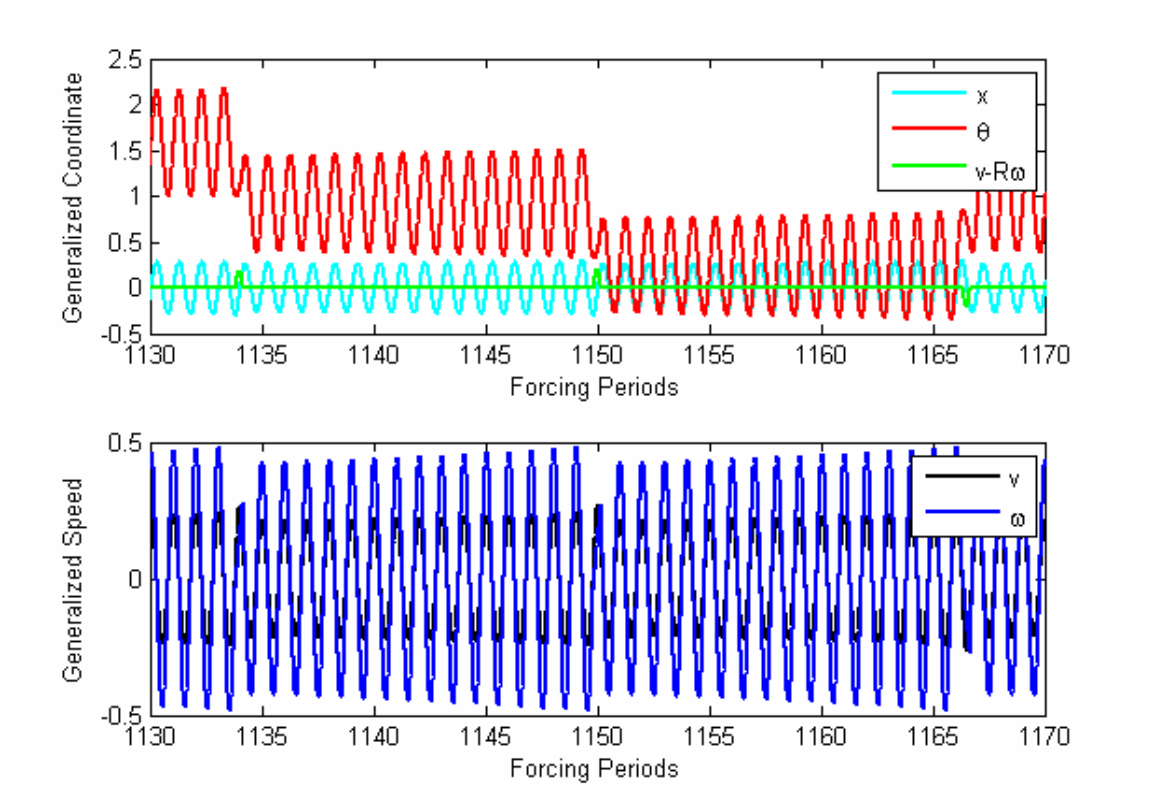

Figure 3-2: The typical roll-slip result for the model. In this case, the mass was set to m=1 kg, the damping was set to c=0.003 N-s/m, the spring constant was set to k=1 N/m, the amplitude of the forcing was set to F=0.003 N, the unstretched spring length was set to L=1 m, the radius of the disk was set to R=0.5 m, the static coefficient of friction was set to μ_s=0.01, the kinetic coefficient of friction was set to μ_k=0.003, and the forcing frequency was set to ω=0.815 rad/s. The simulation was run for 1400 forcing periods, with the first 1000 discarded to avoid transients in analysis.

To further explore the dynamics of the system, the average amplitude of the response over a range of frequencies was found by taking the root-mean-square (RMS) of the signal. The response of the system for the varying values of μ_s over a range of frequencies surrounding the natural frequency, ω_n, is displayed in Figure 3-3. This steady state response includes the response of the system when μ_s=10, resulting in a system that never slips.

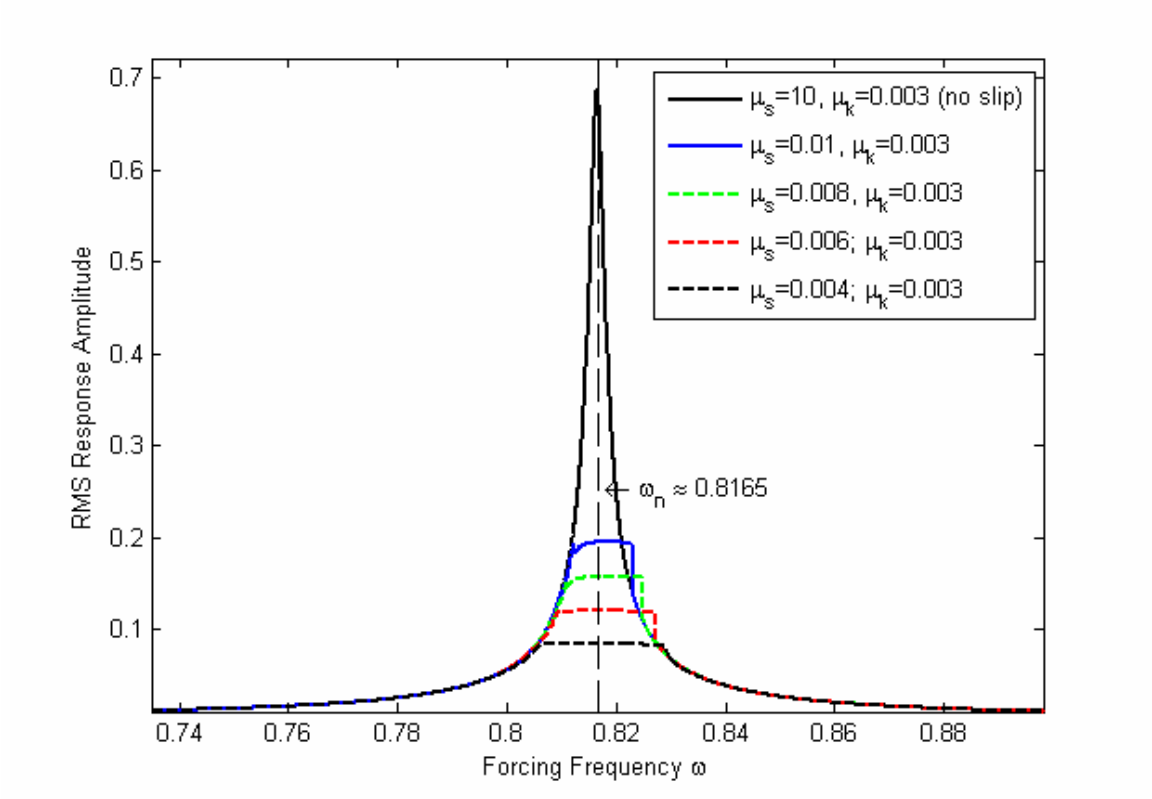

Figure 3-3: The steady state response of the system for varied levels of the static coefficient of friction. In this case, the mass was set to m=1 kg, the damping was set to c=0.003 N-s/m, the spring constant was set to k=1 N/m, the amplitude of the forcing was set to F=0.003 N, the unstretched spring length was set to L=1 m, the radius of the disk was set to R=0.5 m, and the kinetic coefficient of friction was set to μ_k=0.003 while the static coefficient of friction and the forcing frequency were varied. The simulation was run for 1400 forcing periods, with the first 1000 discarded to avoid transients in analysis.

By zooming in on the frequency axis of the plot containing the steady state response, the dynamics occurring within the response can be better observed. In Figure 3-4, the plot of the steady state response has been zoomed in on the frequency axis, displaying the different responses of the system to the varied values of the static coefficient of friction.

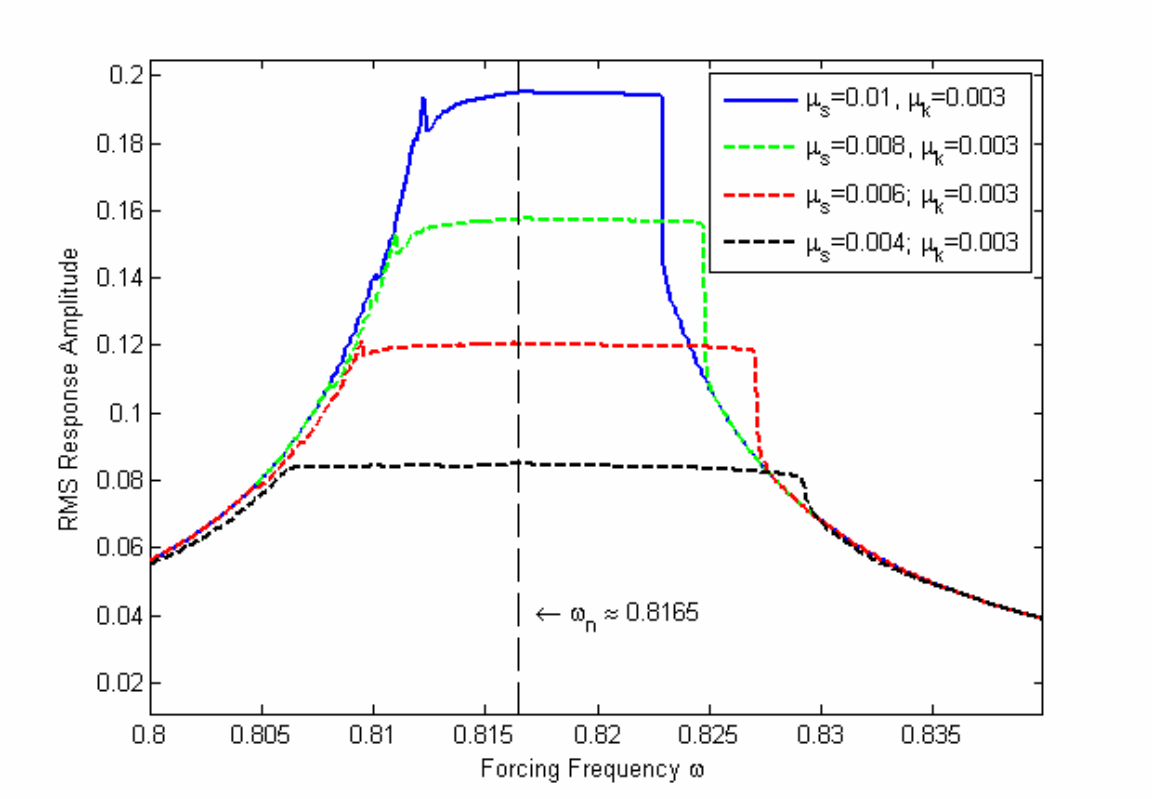

Figure 3-4: The steady state response of the system for varied levels of the static coefficient of friction, zoomed in on the frequency axis. In this case, the mass was set to m=1 kg, the damping was set to c=0.003 N-s/m, the spring constant was set to k=1 N/m, the amplitude of the forcing was set to F=0.003 N, the unstretched spring length was set to L=1 m, the radius of the disk was set to R=0.5 m, and the kinetic coefficient of friction was set to μ_k=0.003 while the static coefficient of friction and the forcing frequency were varied. The simulation was run for 1400 forcing periods, with the first 1000 discarded to avoid transients in analysis.

To better explore the dynamics of the system, the average value of slipping over a range of frequencies was found by again taking the RMS of the signal. The slipping amplitude of the system for the varying values of μ_s over a range of frequencies surrounding the natural frequency, ω_n, is displayed in Figure 3-5.

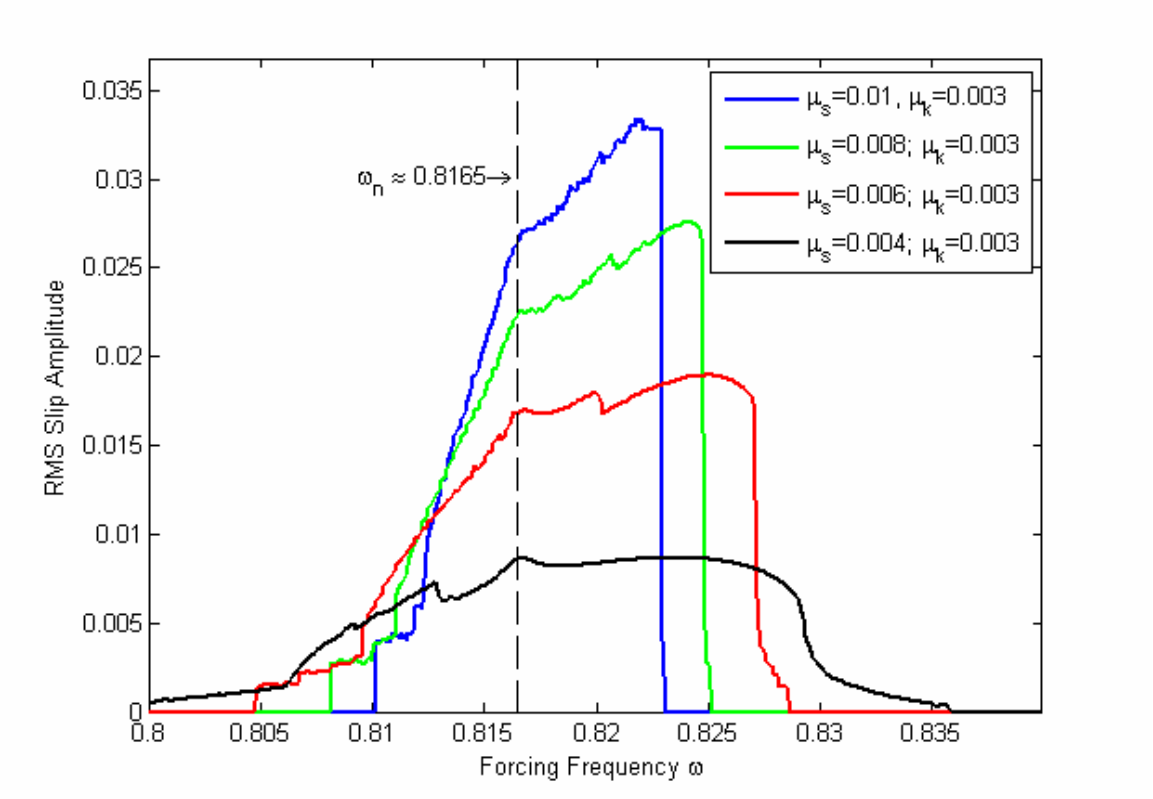

Figure 3-5: The average slipping of the system for varied levels of the static coefficient of friction using RMS. In this case, the mass was set to m=1 kg, the damping was set to c=0.003 N-s/m, the spring constant was set to k=1 N/m, the amplitude of the forcing was set to F=0.003 N, the unstretched spring length was set to L=1 m, the radius of the disk was set to R=0.5 m, and the kinetic coefficient of friction was set to μ_k=0.003 while the static coefficient of friction and the forcing frequency were varied. The simulation was run for 1400 forcing periods, with the first 1000 discarded to avoid transients in analysis.

The last simulation was run to obtain the average power of the system over a range of frequencies by finding the RMS of the signal. The power of the system was found by taking the product of the contact force (P) and the contact velocity (v-$R\omega$) at each time point in the simulation. The average power of the model for varying values of μ_s over a range of frequencies surrounding the natural frequency, ω_n, is displayed in Figure 3-6.

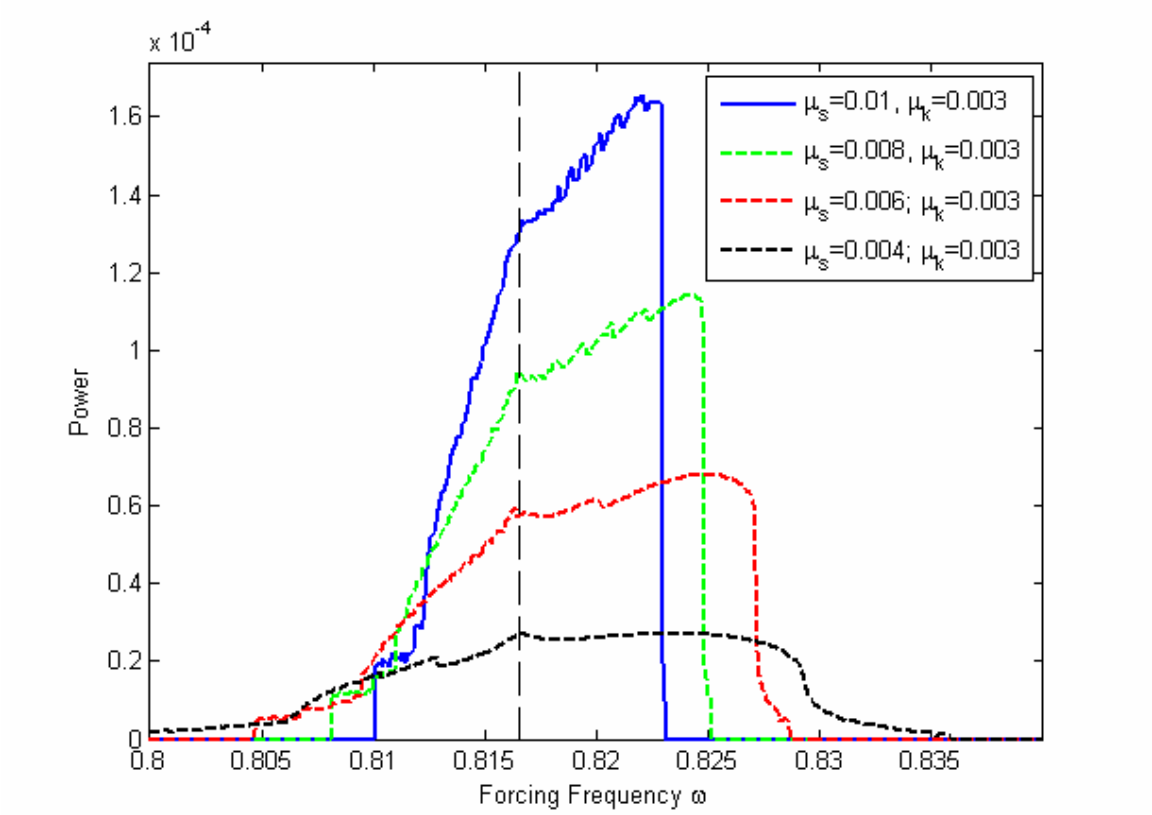

Figure 3-6: The average power of the model. In this case, the mass was set to m=1 kg, the damping was set to c=0.003 N-s/m, the spring constant was set to k=1 N/m, the amplitude of the forcing was set to F=0.003 N, the unstretched spring length was set to L=1 m, the radius of the disk was set to R=0.5 m, and the kinetic coefficient of friction was set to μ_k=0.003 while the static coefficient of friction and the forcing frequency were varied. The simulation was run for 1400 forcing periods, with the first 1000 discarded to avoid transients in analysis.

3.1.2. Discussion

The results in Figure 3-1 show the continuous rolling of the disk, as given by the constant mean value of angular displacement (θ) of the disk as well as by the no slip condition at the point of contact with the surface (v-$R\omega$=0). The roll-slip results in Figure 3-2 show regions of rolling with constant mean values of angular displacement (θ) followed by instances of slipping, denoted by abrupt changes in the mean values of

angular displacement. Slipping is the system is also characterized by peaks or dips in the velocity at the point of contact (v-$R\omega \neq 0$) in the plot. The typical results in Figure 3-1 and Figure 3-2 qualitatively demonstrate the types of motions occurring within the system.

From the results in Figure 3-3, it can be seen that as the static coefficient of friction decreases, the response amplitude caused by the effects of resonance decreases. This is coincident with the effect of slipping; when there is no slipping, it can be noted from the graph that the effects at resonance cause a great displacement. As the static coefficient of friction decreases, the effects of resonance are decreased by the effective capping of the displacement as demonstrated by the RMS response shown in Figure 3-4. From the comparison of Figure 3-3 and Figure 3-4, it is noted that as the static coefficient of friction decreases, the displacement at resonance decreases while the slipping in the system increases.

From the results in Figure 3-5, it can be seen that as the static coefficient of friction decreases, the range of slipping increases while the slip velocity decreases around the resonant frequency. Similarly, from Figure 3-6 it can be noted that as the static coefficient of friction decreases, the power range increases while the value of power in the system decreases around the resonant frequency. Therefore, as the static coefficient of friction decreases, the effects of resonance are decreased by the effective capping of the levels of slipping and power.

Chapter 4

Conclusions and Future Work

4.1. Conclusions

Based on the results obtained from the system, it can be concluded that as the static coefficient of friction increases, the displacement and average power of the disk increase while the slipping of the disk decreases. In other words, slipping within the system aids in reducing the response amplitude and the increased level of power caused by resonance effects. Slipping acts to effectively cap the steady state response and average power amplitudes occurring around the resonant frequency, dampening the effects of resonance in the system.

Biologically speaking, if a surface change occurs within the knee that increases the static coefficient of friction between the articular surfaces and the menisci, slipping would be decreased which would decrease the efficiency of motion of the knee while increasing the effects of resonance. An example of this phenomenon is a meniscal tear in the medial or lateral meniscus, increasing the static coefficient of friction in the joint. As a result, the response amplitude would increase; biologically, the femur will have greater displacement on the tibia. The power would also increase; biologically, the femur will cause more wear on the joint surface. Both of these phenomena would result in increased joint instability and potentially lead to serious injury of the joint, such as torn ligaments or bone-on-bone contact within the joint. Therefore, slipping is a key factor in knee stability. Low slip velocities are desirable, as concluded by Schwenke, et al.; however, in

addition to the actual value of slipping, a wide range of slipping in the system is important in controlling the dynamic response to resonance within the knee.

Similarly, a low level of power within the joint in combination with a wider range is important in minimizing the generation of wear. Biologically speaking, a meniscal tear that increases the static coefficient of friction would result in higher values of power within the joint, increasing the wear on the surface. The increased wear would further exacerbate the increased static coefficient of friction, as well as affect other dynamical aspects of the joint, including slipping. Overall, maintaining a static coefficient of friction approximately equal to the kinetic coefficient of friction in the knee will lead to the adequate slipping and low levels of power within the knee joint that are necessary for ensuring stability and integrity of the joint.

4.2. Future work

For future work on this model, a more in-depth analysis should be performed on the dynamical response of this system to give better insight into frequency content and periodicity. More specifically, the regions inside of slipping should be examined to further explore roll-slip transitions, as well as system characteristics during slipping. In addition, the jumps of the plots off the main graph lines in Figure 3-1 should be investigated. Although these are thought to be associated with noise in the system, which is also a biological phenomenon, this should be confirmed through further analysis.

To further the current model for more realistic applications, the flat surface should be replaced by a curved surface to better replicate a biologically realistic knee. In adding a curved surface, the equations for analysis become much more complex as the normal

force changes as a function of position on the curved surface. This complexity could easily lead to interesting dynamical results as other factors besides the static coefficient of friction will contribute to system response, which could provide insight into biological events occurring within the knee, from regular walking motions to soft tissue injuries. The spring constant and damping factors could also be examined to obtain information regarding the role of soft tissues within the knee joint and the instability resulting from weakened ligaments. These factors should be thoroughly explored to gain more insight into the dynamics occurring during various states and motions of the knee.

References

[1] Seebacher, J. R., Inglis, A. E., Marshall, J. L., and Warren, R. F., 1982, "The Structure of the Posterolateral Aspect of the Knee," Journal of Bone and Joint Surgery-American Volume, 64(4), pp. 536-541.

[2] Andriacchi, T. P., 1996, "Gait analysis and total knee replacement," Current Concepts in Primary and Revision Total Knee Arthroplasty, pp. 29-36;286.

[3] Martini, F., and Ober, W. C., 2006, Fundamentals of anatomy & physiology, Pearson Benjamin Cummings, San Francisco, CA.

[4] Martin, H. N., and Martin, E. G., 1926, The human body: its structure and activities and the conditions of its healthy working, H. Holt and Co., New York.

[5] Krames, C., "Knee Joint." http://www.orthopaedics.co.uk/boc/patients/knee_arthritis_intro.htm.

[6] Martini, F., and Ober, W. C., 2006, Martini's atlas of the human body, Pearson/Benjamin Cummings, San Francisco.

[7] Watkins, J., 1999, Structure and function of the musculoskeletal system, Human Kinetics, Champaign, IL.

[8] Garden, R. S., 1961, "The Structure and Function of the Proximal End of the Femur," Journal of Bone and Joint Surgery-British Volume, 43(3), pp. 576-589.

[9] NIH, 2009, "Anterior cruciate ligament (ACL) injury," http://www.nlm.nih.gov/medlineplus/ency/article/001074.htm.

[10] Awrejcewicz, J., and Someya, T., 1992, "A Twisted Horseshoe in the Roll-Slide Oscillator," Journal of the Physical Society of Japan, 61(5), pp. 1556-1559.

[11] Schwenke, T., Borgstede, L. L., Schneider, E., Andriacchi, T. P., and Wimmer, M. A., 2005, "The influence of slip velocity on wear of total knee arthroplasty," Wear, 259, pp. 926-932.

[12] Mayo Clinic, "ACL Injury."

[13] Herr, H., and Wilkenfeld, A., 2003, "User-adaptive control of a magnetorheological prosthetic knee," Industrial Robot-an International Journal, 30(1), pp. 42-55.

[14] Andriacchi, T. P., Galante, J. O., and Fermier, R. W., 1982, "The Influence of Total Knee-Replacement Design on Walking and Stair-Climbing," Journal of Bone and Joint Surgery-American Volume, 64(9), pp. 1328-1335.

[15] Hafner, B. J., and Smith, D. G., 2009, "Differences in function and safety between Medicare Functional Classification Level-2 and-3 transfemoral amputees and influence of prosthetic knee joint control," Journal of Rehabilitation Research and Development, 46(3), pp. 417-433.

[16] Keinath, B., "Demonstrating Altered Kinematics from Ligament Injuries with a Three Dimensional Knee Model," Union College, Schenectady, p. 20.

[17] Srinivasan, M., and Ruina, A., 2006, "Computer optimization of a minimal biped model discovers walking and running," Nature, 439(7072), pp. 72-75.

[18] Hibbeler, R. C., 2007, Engineering Mechanics: Dynamics, Pearson/Prentice Hall, Upper Saddle River.
[19] Feeny, B., and Moon, F. C., 1994, "Chaos in a Forced Dry-Friction Oscillator - Experiments and Numerical Modeling," Journal of Sound and Vibration, 170(3), pp. 303-323.
[20] Boyce, W. E., and DiPrima, R. C., 2005, Elementary differential equations and boundary value problems, Wiley, Hoboken, NJ.
[21] MathWorks, "MATLAB - The Language of Technical Computing," http://www.mathworks.com/products/matlab/.
[22] Roy, A., 2010, "roll_slip_disk_v5.m" University Park, MATLAB code to model slip-roll motions in a damped oscillator.
[23] Herman, I. P., and SpringerLink (Online service), 2007, "Physics of the Human Body," Biological and Medical Physics, Biomedical Engineering,, Springer-Verlag Berlin Heidelberg, Berlin, Heidelberg.

Appendix A

Algorithm Logic

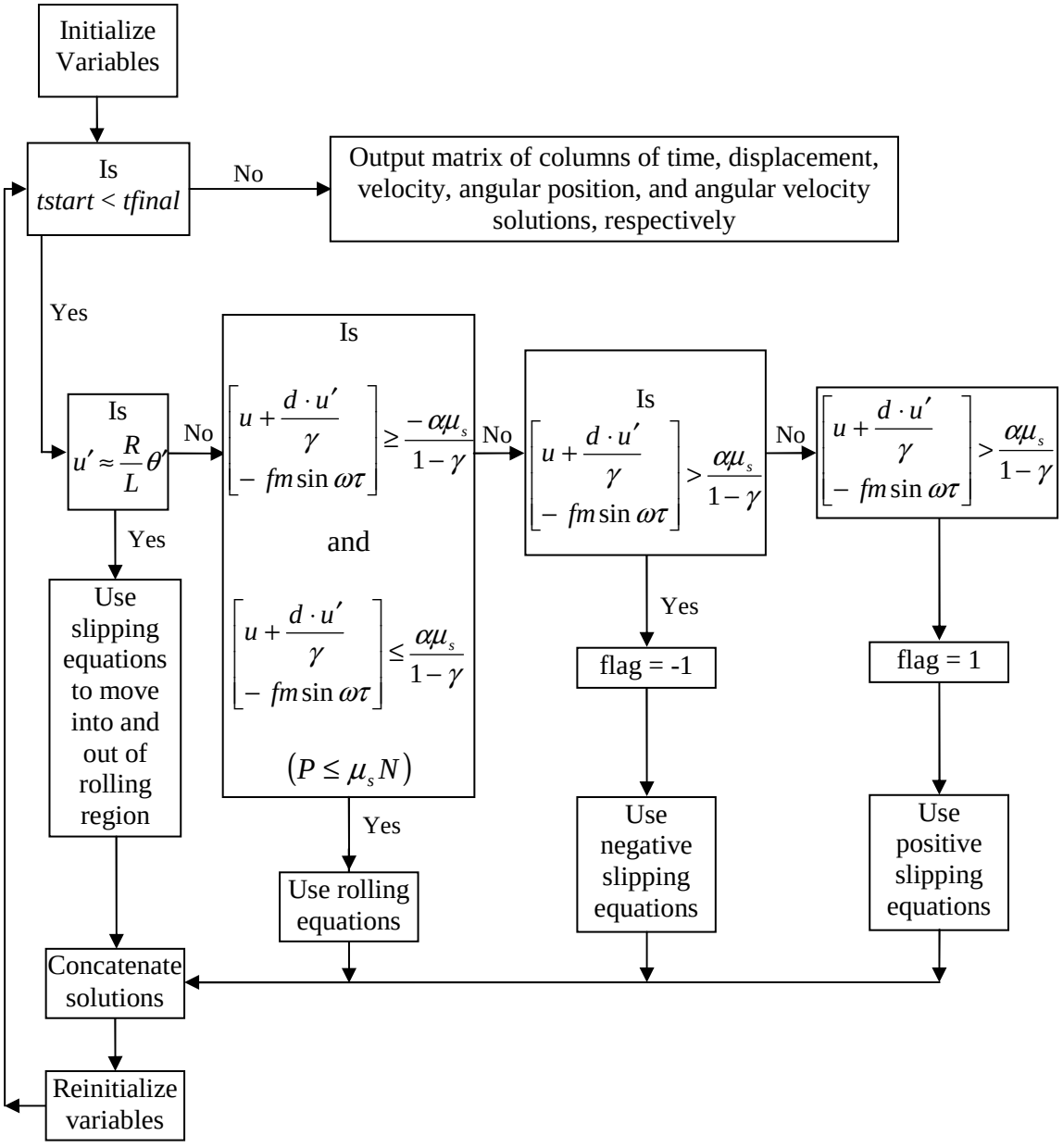

Virginia Gagliardi

— vmg5007@psu.edu —

Current Address:

820 Cricklewood Dr., Apt. 101
State College, PA 16803
484.347.9279

Academic Vita

Permanent Address:

4197 Salem Drive
Emmaus, PA 18049
610.928.0073

EDUCATION

Undergraduate — The Pennsylvania State University, University Park — May 2010
The Schreyer Honors College
B.S. in Bioengineering with honors in Bioengineering
GPA: 3.96/4.0

THESIS

Undergraduate — Modeling the Roll-Slip Nonlinear Dynamics of the Knee
Supervisor: Professor Joseph P. Cusumano

WORK EXPERIENCE

Research — Nonlinear Dynamics Lab — January 2008-May 2010
The Pennsylvania State University
Supervisor: Professor Joseph P. Cusumano

- Modeled the internal dynamics of the knee in order to gain insight into the relative motions of the knee joint
- Simulated dynamic models utilizing MATLAB programming to analyze periodic motions of the knee and the potential significance in clinical applications
- Research culminated in a final thesis defended in Spring 2010

Internship — Validation Group — February 2009-July 2009
MedImmune, Frederick, MD
Supervisors: Alison Demarest and Tom Blake

- Executed Factory Acceptance Testing (FAT) on operational sequences of CIP pathways through PCS simulation
- Utilized P&IDs to obtain relevant data to generate PQ protocols for SIP and CIP of product tanks and process lines

- Generated and obtained approval of Master Calibration Records for over 1200 product-critical instruments in the facility

Internship — Validation Group — August 2008-January 2009
Novavax, Inc., Rockville, MD
Supervisor: Niclas Bogren

- Authored validation documents and standard operating procedures for cGMP operations
- Executed validation protocols on facility equipment, including performing temperature mapping with the Kaye Validator
- Drafted process diagrams for scale-up process collaborators and for presentation to CFO
- Assisted in aseptic sampling while gaining knowledge of bioreactor culture, filtration, and process management

Research — Physics Lab — January 2007-August 2007
The Pennsylvania State University
Supervisor: Associate Professor Leonard P. Gamberg

- Analyzed quark movement and existence of transverse spin and momentum
- Utilized tools like Mathematica and Fortran to write and analyze structure functions
- Presented beginnings of work at an Undergraduate Research Conference

Internship — Drafting — May 2006-August 2006
CRG Energy Consultants
Supervisor: C. Gagliardi

- Assisted in designing energy flowcharts
- Checked scaling on floor and building plans for The Beech Hollow Project (description available upon request)
- Observed the technical abilities associated with engineering while assisting with a $650 million power plant project

Private Tutor — Algebra and Trigonometry — October 2005-April 2006
Annville, PA

- Provided academic support in the field of mathematics to a high school student
- Focused on improvement in weak areas leading to increases of 35% in grade reports

Private Tutor | Algebra | September 2004-June 2005
Emmaus, PA

- Provided learning support in the field of mathematics to a middle school student
- Prepared bi-weekly analyses on academic performance of student to identify weaknesses
- Increased student understanding leading to grade improvement by 40%

DESIGN PROJECTS

Humanitarian | The HeartThrob Stethoscope | February 2010-April 2010

- Worked on humanitarian engineering project to bring pre-primary healthcare to rural regions of Africa using telemedicine
- Designed low-cost electronic stethoscope with the design goal to record heart and lung sounds in noisy kiosk environment
- Cost of final design was under $10
- Device to be tested in Kenya with the Mashavu system in the summer of 2010

Humanitarian | Mashavu Eyecare System | January 2010-April 2010

- Worked on advanced humanitarian engineering project to bring basic healthcare to rural regions of Africa using telemedicine
- Designed low-cost, versatile eye camera to capture images of the inside of the eye
- Cost of final design was under $150
- Final design to be submitted to the NCIIA BMEStart competition in May 2010

PUBLISHINGS AND PRESENTATIONS

Gagliardi, Virginia. "Left Out." *Sticks and Stones and Other Student Essays*. Ed. Ruthe Thompson and Charles R. Cooper. Boston: Bedford/St. Martin's, 2007. Print.

Gagliardi, Virginia. "Quark Behavior in Relation to Characteristics of the Proton." The Undergraduate Research Conference. The Pennsylvania State University, Berks Campus, Reading. 21 Apr. 2007.

HONORS AND AWARDS

Honor Societies	Tau Beta Pi Phi Kappa Phi National Society of Leadership and Success Golden Key International Honor Society
Scholarships	ALCOA Engineering Scholarship Phi Sigma Delta Scholarship University Trustee Scholarship Mathias Scholarship Smidansky Family Scholarship
Awards	First Place, FYS Writing Contest, Lebanon Valley College Dean's List (All Semesters) WEP—Priscilla Guthrie Award, Honorable Mention

LEADERSHIP

Candidate Mentor	Tau Beta Pi The Pennsylvania State University	2009-Present
Chapter Founder	AEMB Honor Society (Future Candidate Chapter) The Pennsylvania State University	2009-Present
Panel Speaker	First Year Seminar Bioengineering Classes The Pennsylvania State University	2007-Present
Volunteer	Centre County PAWS Centre County, PA	2007-Present

PROFESSIONAL MEMBERSHIPS

- BMES (2008, 2010)
- SWE (2007-2009)
- PDA (2008-2009)
- ISPE (2008-2009)